Effect of controlled crystallization on polaronic transport in phosphate-based glass-ceramics

Pavić, Luka; Nikolić, Juraj; Graça, Manuel P. F.; Costa, Benilde F. O.; Valente, Manuel A.; Skoko, Željko; Šantić, Ana; Moguš- Milanković, Andrea

Source / Izvornik: **International Journal of Applied Glass Science, 2020, 11, 97 - 111**

Journal article, Published version
Rad u časopisu, Objavljena verzija rada (izdavačev PDF)

https://doi.org/10.1111/ijag.13618

Permanent link / Trajna poveznica: https://urn.nsk.hr/urn:nbn:hr:217:140991

Received: 31 May 2019 | Revised: 1 August 2019 | Accepted: 22 August 2019

DOI: 10.1111/ijag.13618

INTERNATIONAL JOURNAL OF Applied Glass SCIENCE

SPECIAL ISSUE ARTICLE

Effect of controlled crystallization on polaronic transport in phosphate-based glass-ceramics

Luka Pavić[1] | **Juraj Nikolić**[1] | **Manuel P.F. Graça**[2] | **Benilde F.O. Costa**[3] | **Manuel A. Valente**[2] | **Željko Skoko**[4] | **Ana Šantić**[1] | **Andrea Moguš-Milanković**[1]

[1]Division of Materials Chemistry, Ruđer Bošković Institute, Zagreb, Croatia

[2]I3N, Physics Department, University of Aveiro, Aveiro, Portugal

[3]CEMDRX, Physics Department, University of Coimbra, Coimbra, Portugal

[4]Department of Physics, Faculty of Science, University of Zagreb, Zagreb, Croatia

Correspondence
Andrea Moguš-Milanković, Ruđer Bošković Institute, Zagreb, Croatia
Email: mogus@irb.hr

Funding information
Croatian Science Foundation, Grant/Award Number: IP-09-2014-5863 and 03.01/156; Ministry of Science, Education and Sport of the Republic of Croatia, Grant/Award Number: 098–0982929-2916 and PEst-C/CTM/LA0025/2011

Abstract

The effect of induced crystallization on changes in electrical transport of two types of glass-ceramics, pure polaron conductive $40Fe_2O_3$-$60P_2O_5$ (F40) (mol%) and predominantly polaronic $5Li_2O$-$5ZnO$-$40P_2O_5$-$50WO_3$ (Li-50W) (mol%) was investigated. F40 glass-ceramics produced at low heat-treatment temperatures contain single-phase $Fe_3(P_2O_7)_2$ whereas at higher temperatures two more phases $Fe_4(P_2O_7)_3$ and $Fe(PO_3)_3$ are formed. Structural modifications strongly depend on the crystallization temperature and time. The appearance of crystalline phases studied by Mössbauer spectroscopy exhibits changes in Fe^{2+}/Fe_{tot} ratio in crystalline/glassy phases. The detailed analysis of different iron sites allows their correlation with changes in electrical conductivity as crystallization progresses. Depending on the course of crystallization, the contribution of each phase to the overall conductivity is determined by the frequency dependence of $Z''(\omega)$ and $M''(\omega)$. DC conductivity shows a sharp decrease as $Fe_3(P_2O_7)_2$ phase appears and consequently glass matrix remains impoverished in Fe^{2+}-Fe^{3+} pairs. In the multiphase systems prepared at higher crystallization temperatures, the overall electrical conductivity increases although the continuous grain boundaries along different crystalline grains play a limiting factor. In contrast, the slight conductivity change in Li-50W glass-ceramics upon crystallization is a result of remaining W^{5+}-W^{6+} pairs in the residual glassy phase. Independence of electrical transport on Li^+ ions confirms predominantly polaronic transport in Li-50W glass-ceramics.

KEYWORDS

glass ceramics, induced crystallization, iron phosphate glass, Mössbauer spectroscopy, polaronic transport, structural properties

1 | INTRODUCTION

The recently revised definition of glass-ceramics states that the glass-ceramics are inorganic, nonmetallic materials prepared by controlled crystallization of glasses via different processing methods. They contain at least one type of functional crystalline phase and a residual glass.[1] The transformation from glass to glass-ceramics takes place by a controlled process of nucleation and crystals growth giving rise to the evolved nano- and microstructures.[2,3] Properties of glass-ceramics are strongly dependent on size, type, morphology and distribution of crystalline phases inside the glass

matrix which offer vast possibilities for the development of these materials in diverse fields of applications.

In the past few years, the interest in investigating phosphate glasses and glass-ceramics has been increased. It is well known that phosphate-based glasses are interesting from a scientific and technological point of view due to their low melting temperature, high thermal expansion coefficient, and high ultraviolet transmission.[4,5] On the other hand, their poor chemical durability can be significantly enhanced by the addition of the various transition metal oxides (TMO) such as Fe_2O_3, MoO_3, or WO_3.[6–9] As a result, these glass systems are not just highly chemically durable, but also act as electronically conducting glasses with polaronic conduction mechanisms.[10–17]

Among various TMO-phosphate glass systems, iron phosphates are best known for their exceptional chemical durability and high solubility of various nuclear waste compounds which sets the direction of their application as a host material for vitrification of nuclear wastes.[18] In particular, it has been reported that the glass of molar composition $40Fe_2O_3$-$60P_2O_5$ shows the best combination of high chemical durability[7,19] and low crystallization tendency.[7,20]

The focus of so far published studies on induced crystallization of iron phosphate glasses was mainly on the structural changes which depend on glass composition and crystallization conditions but less on their influence on the electrical transport.[8,21–25] Our recent investigations, however, show that the controlled crystallization appears to be a powerful tool for tailoring electrical properties of these materials.[26,27] For instance, our study on the $10ZnO$-$30Fe_2O_3$-$60P_2O_5$ (mol%) glass system[26] shows that in the initial stage of crystallization, the electrical conductivity decreases, whereas with further crystallization progress it rises as a consequence of an increase in the size of crystal grains and their different distribution within the glass matrix. Further, our investigation on the electrical properties of $40Fe_2O_3$-$60P_2O_5$ (mol%) glass-ceramic[27] reveals that the thermally induced microstructural changes and the formation of various crystalline phases have a significant impact on electrical transport. In this glass-ceramic system, different electrical processes could be identified and their contribution to the overall electrical conductivity could be determined.[27]

Another TMO which is very important for phosphate glasses is tungsten oxide. Several studies have shown that the addition of higher amounts of WO_3 to phosphate glass leads to high thermal stability against crystallization and high glass transition temperatures.[28–30] These properties are found to be strongly related to the incorporation of WO_3 into phosphate glass.[29–34] Moreover, glasses with high WO_3 content contain clusters of WO_6 octahedra which play a key role in polaronic transport mechanism making these glasses highly conductive.[31,32]

Wide compositional flexibility of phosphate glasses offers a possibility to combine ionic conduction with polaronic transport by the introduction of highly mobile cations such as Li^+, Na^+, and Ag^+ ions into TMO-phosphate systems. In such mixed ion-polaron glasses, the polaronic contribution arises from the polaron hopping between transition metal ions in different oxidation states,[11,12] whereas the ionic conductivity is a result of the monovalent cations migrating through the glass network.[35,36] From the technological point of view, mixed ion-polaron conduction is highly important for the cathode materials in batteries[37,38] since the best performance is achieved when ionic transport is less than twice in magnitude than the polaronic one.[39,40] While in glassy systems contributions of polaronic and ionic conductivity can be controlled by the glass composition and structure, the thermally induced crystallization represents an advantageous procedure for developing new ion-polaron materials due to the possibility of fine-tuning their electrical properties via microstructural changes.[41,42]

Most recently, we have investigated electrical transport in zinc phosphate glasses which contain alkali[31] and silver[32] oxides in combination with WO_3. The study revealed that the systematic replacement of $Li_2O/Na_2O/Ag_2O$ by WO_3 results in a sharp minimum in DC conductivity, which indicates a transition from predominantly ionic to predominantly polaronic conductivity. This result implies that these glass systems contain significant contributions of two types of charge carriers, ions, and polarons, which can both participate in the conduction process making these glasses prospective mixed conductors.

Considering the crystallization processes in phosphate glasses containing WO_3, there are numerous reports on binary tungsten phosphate and tungsten fluorophosphate glass-ceramics, and their optical properties.[43–46] However, reports on controlled crystallization of tungsten phosphate glasses containing alkali oxide are very rare.[47]

The aim of this work was to systematically examine the effect of the controlled crystallization on the electrical conductivity of two glass systems: (i) pure polaron conductive $40Fe_2O_3$-$60P_2O_5$ (mol%) and (ii) predominantly polaron conducting $5Li_2O$-$5ZnO$-$40P_2O_5$-$50WO_3$ (mol%). The crystallization of the former system was controlled by varying both heat-treatment temperature and time in a wide range, for 1, 6, 12, and 48 h, which allowed us to correlate and supplement the results with our previous study on this system crystallized at different temperatures for 24 hours.[27] On the other hand, crystallization of the latter glass system was achieved by heat treatment at different temperatures for 1 and 6 h. Such variations of the heat-treatment conditions enabled us to prepare glass-ceramics with different types and amounts of crystalline phases and to comprehensively investigate their roles in the electrical transport. Overall, this research provides a novel insight into the changes in electrical properties

and contributes to a better understanding of mechanisms of charge transfer in the pure electronic and predominantly polaronic glass-ceramics.

2 | MATERIALS AND METHODS

2.1 | Parent glasses and glass-ceramics preparation

A detailed preparation procedure of the parent glasses of molar composition $40Fe_2O_3$-$60P_2O_5$ (F40) and $5Li_2O$-$5ZnO$-$40P_2O_5$-$50WO_3$ (Li-50W) has been reported in Refs. [27] and [31], respectively.

Both F40 and Li-50W parent glasses were prepared by standard melt-quench technique. Reagent grade materials for F40 glass were melted for 2 h at 1150-1200°C in Al_2O_3 crucibles. Afterward, melts were poured into preheated molds in the shape of long bars and annealed for 4-6 h in air at 450°C and then cooled to room temperature. On the other hand, reagent grade materials for Li-50W glass were melted at 1350°C in ambient air and then poured into a circular graphite mold. Obtained Li-50W glass was annealed for 3 h at 463°C and slowly cooled to room temperature. Prepared glasses were transparent being black in case of F40 and deep blue for Li-50W, see Figure S1 in Supporting Information.

The amorphous character of the glass samples was confirmed by Powder X-ray Diffraction (PXRD) analysis. The fraction of iron ions in different oxidation states, namely as Fe^{2+} and Fe^{3+}, in two prepared glass bars of F40 composition was determined by Mössbauer spectroscopy. We found that for one glass bar the Fe^{2+}/Fe_{tot} fraction was 0.16, whereas for another it was 0.18. The observed difference is due to the fact that Fe^{2+}/Fe_{tot} fraction is highly sensitive to the melting conditions.[23] However, since it is expected that such slight difference does not affect the crystallization process nor the electrical properties of as-prepared glass-ceramics, we have used both glass bars in further investigation; glasses from the first bar with 16% of Fe^{2+} were subjected to structural characterization of glass-ceramics by means of Mössbauer spectroscopy and those from the second bar where the concentration of Fe^{2+} was 18% were used for electrical characterization of glass-ceramics.

The fraction of tungsten ions in different oxidation states, namely as W^{5+} and W^{6+}, in Li-50W glass was determined from the magnetization measurements using SQUID magnetometer. [31] The fraction of W^{5+} was found to be 1.26%.[31]

The glass transition temperature, T_g, and crystallization temperature(s), T_c, for F40 and Li-50W glasses were determined from their DTA and DSC curves, respectively. It is well known from the literature that F40 glass has a T_g at ≈520°C, and exhibits two wide exothermic peaks at ≈650 and ≈800°C that correspond to the crystallization temperatures.[23] The first exothermic peak which extends through a broad temperature range from 550 to 700°C is attributed to $Fe_3(P_2O_7)_2$, while the second one, which extends through somewhat narrower temperature range from 750 to 830°C, corresponds to $Fe_4(P_2O_7)_3$.[23] It should be pointed out that even though the as-prepared F40 glasses contain slightly different Fe^{2+} concentration either 18% or 16%, the crystalline phases obtained in heat treatments are the same. Also, the temperatures of their emergence are slightly shifted, see Figure S2 in Supporting Information, but that does not influence the overall crystallization processes.

For Li-50W glass, the thermal events were determined from DSC measurements which were performed on powder samples (100 mg) with a diameter of ≈10 μm placed in an open platinum crucible under flowing nitrogen atmosphere at a heating rate of 10°C min^{-1}. The DSC curve shows T_g at approximately ≈470°C and two wide exothermic peaks with centers at ≈600 and ≈725°C, see Figure S3.

The induced crystallization of the parent F40 and Li-50W glasses was performed by thermal treatments of the samples in the form of ≈1-mm thick disks at controlled temperatures and times. F40 glasses were heated in Barnstead Tube Furnace 21100, with 10°C min^{-1} in steady air atmosphere up to the selected temperature (530, 560, 590, 620, 670, 720, 770, 800°C) and held at that temperature for various times (1, 6, 12, 24, and 48 h).

The controlled crystallization of Li-50W glasses was performed in Nabertherm furnace by heating the sample with 10°C min^{-1} in steady air atmosphere up to the selected temperature (600, 725 and 800°C) at which the sample was held for 6 h.

In this manuscript, the as-prepared glass-ceramics are labeled in accordance with their glass composition and crystallization time and temperature. For example, the sample F40-6@720 is prepared by heat treatment of F40 glass at 720°C for 6 h.

2.2 | Glass-ceramics characterization

PXRD patterns of prepared glass-ceramics were collected at room temperature (RT) by Philips automatic diffractometer in Bragg-Brentano geometry. In the experiment, Cu K_α radiation was used at 40 kV and 30 mA (PW 1820 model) and 45 kV and 40 mA (X'Pert MPD model). Intensity data were obtained in the 2θ angle range from 10 to 70º, with the step of 0.02º. Crystalline phase identification was done using the ICDD-PDF database. The amount of the crystalline phases was determined by the Rietveld method using an internal standard, ZnO powder.[27] Rietveld analysis was performed with commercial software X′Pert HighScore (Plus).

The microstructure of the glass-ceramics was studied by Scanning Electron Microscopy FE-SEM JSM 7000 (JEOL).

Samples were not coated with an electrically conductive layer and the accelerating voltage was kept low.

^{57}Fe Mössbauer spectra were collected to characterize the valence state of iron ions and their coordination environment in the F40 glass-ceramic structures. The spectra were recorded at RT in transmission geometry in a constant acceleration type spectrometer using a ^{57}Co/Rh source with a strength of 20 mCi. The fitting of the spectra was carried out with a set of Lorentzian lines, determined by least squares minimization. The isomer shifts were referenced to α-Fe at RT.

Electrical properties were studied by Impedance spectroscopy (IS). The gold electrodes were sputtered onto both sides of ≈1-mm thick sample disks using Sputter coater SC7620. Complex impedance, Z^*, was measured using an impedance analyzer (Novocontrol Alpha-AN Dielectric Spectrometer, Novocontrol Technologies GmbH & Co.) over the frequency range from 0.01 Hz to 1 MHz at temperatures between 30 and 250°C. The temperature was controlled to an accuracy of ± 0.2 K. The data were analyzed using three interrelated formalisms: complex impedance, Z^*, complex electrical modulus, M^*, and complex conductivity, σ^*.

3 | RESULTS AND DISCUSSION

3.1 | Polaron glass-ceramics

3.1.1 | Structure of iron phosphate glass-ceramics

According to the DTA results, the temperatures of heat treatments of F40 glass are set to be in the temperature region between 530 and 800°C.[24,27] Duration of heat treatment at each temperature (530, 560, 590, 620, 670, 720, 770, 800°C) varies from 1, 6, 12, 24 to 48 hours. It was previously reported[23–25,27] that the three crystalline phases, namely $Fe_3(P_2O_7)_2$ (PDF No: 01-080-2315), $Fe_4(P_2O_7)_3$ (PDF No: 01-073-6768), and minor $Fe(PO_3)_3$ (PDF No: 01-089-8524) are created during crystallization. The appearance of each crystalline phase in the glass matrix depends on the time and temperature of heat treatment.

Figure 1 shows the PXRD patterns for F40 glass and glass-ceramics heat-treated at various temperatures for 6 and 48 hours. For F40 glass crystallized for 6 hours at 530 and 560°C, the PXRD patterns are free of diffraction lines showing a wide *halo* which confirms the amorphous state. With increasing heating temperatures up to 770°C, the diffraction lines that correspond to the pyrophosphate $Fe_3(P_2O_7)_2$ crystalline phase appear, while at 800°C the beginning of the formation of the second crystalline phase $Fe_4(P_2O_7)_3$ is detected. The PXRD patterns for glass-ceramics prepared by heat treatments for 48 hours show diffraction lines related to the $Fe_3(P_2O_7)_2$ in the temperature range from 560 to 720°C. Furthermore, the increase in crystallization temperatures to 770 and 800°C results in the additional diffraction lines characteristic for $Fe_4(P_2O_7)_3$ and $Fe(PO_3)_3$ phases. It should be noted that the heat treatment at higher temperatures causes a massive crystallization, which leads to the presence of all three crystalline phases embedded in a minor residual glassy phase. The appearance of the detected crystalline phase(s) is in accordance with the literature data.[23–25,27]

The dependence of total crystallinity upon heat-treatment temperatures and times calculated using Rietveld analysis is exhibited in Figure 2. Generally, with increasing heat-treatment temperature and time, total amount of crystalline

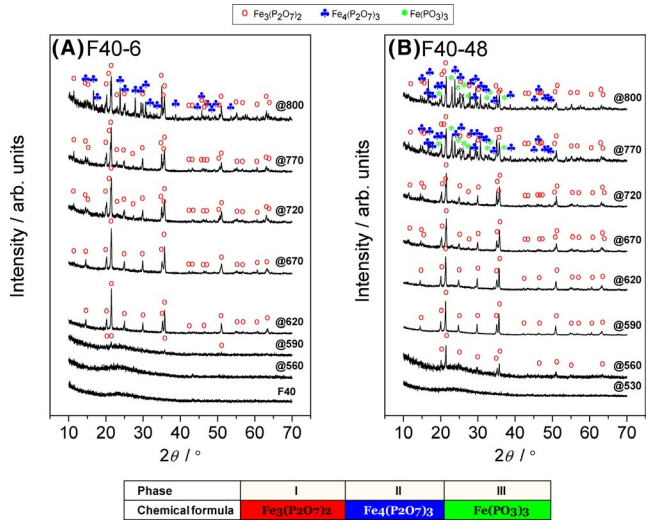

FIGURE 1 PXRD patterns for F40 glass and glass-ceramics heat-treated at various temperatures for (A) 6 and (B) 48 h. In glass-ceramics heat-treated at 770 and 800°C for 48 h, an indication of $FePO_4$ phase is observed and marked with symbol X (diffraction line at $2\theta = 25.9°$)

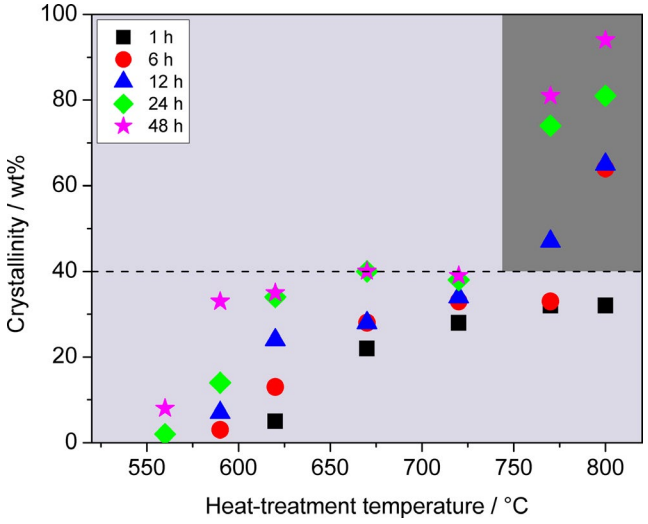

FIGURE 2 Dependence of the crystallinity upon the heat-treatment temperatures for various heat-treatment times for F40 glass-ceramics

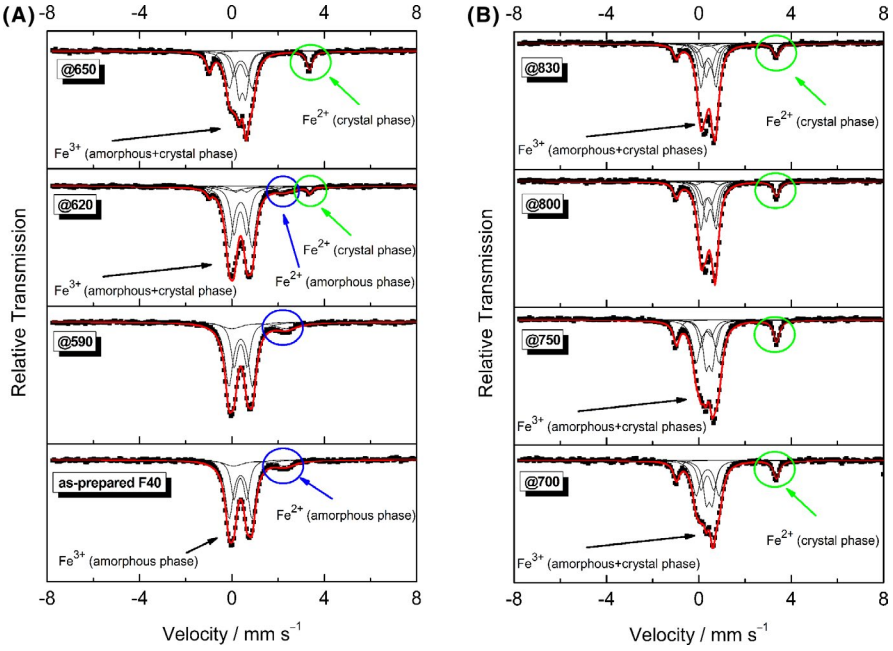

FIGURE 3 Mössbauer spectra of starting F40 glass and glass-ceramics prepared by heat treatment at various temperatures for 24 h

phase(s) increases. However, it is interesting to note that within the range of single crystalline phase, that is, up to 720°C, see Figure 1, the amount of $Fe_3(P_2O_7)_2$ increases with both time and temperature and reaches maximal value of 40 wt% (marked as a black-dashed line in Figure 2). Also, it should be noted that with increasing duration of heat treatments in this temperature range, the formation of $Fe_3(P_2O_7)_2$ phase is shifted to the lower temperatures. For example, for F40-1 the $Fe_3(P_2O_7)_2$ appears at 620°C while for F40-48, it is formed at 560°C. In the temperature region of 770-800°C, crystallinity sharply increases as a result of the formation of $Fe_4(P_2O_7)_3$ and $Fe(PO_3)_3$, see Figures 1 and 2.

Going further into the structural analysis it is important to point out that $Fe_3(P_2O_7)_2$ contains both Fe^{2+} and Fe^{3+} ions where Fe^{2+} is in a specific trigonal prismatic coordination.[48] In contrast, both $Fe_4(P_2O_7)_3$ and $Fe(PO_3)_3$ contain only Fe^{3+} ions.[49] Changes in the concentrations of Fe^{2+} and Fe^{3+} ions in the glass-ceramics are especially important for the interpretation of electrical properties.

3.1.2 | Mössbauer spectroscopy

In order to determine the progress of the crystallization and changes in Fe^{2+}/Fe_{tot} ratio of F40 glass-ceramics, Mössbauer spectroscopy was used. The room temperature ^{57}Fe Mössbauer spectra of starting F40 glass which contains 16% of Fe^{2+} ions and F40 glass-ceramics prepared by heat treatment for 24 hours are shown in Figure 3.

The Mössbauer hyperfine parameters, isomer shift, δ, quadrupole splitting, Δ, line width Γ, and a fraction of Fe^{2+} are listed in Tables 1 and 2. Mössbauer spectra of starting F40 glass and sample heat-treated at 590°C are similar and can be decomposed into three sets of doublets using Lorentzian shapes. These doublets represent one doublet of Fe^{2+} in an octahedral site and two central superimposed doublets related to the Fe^{3+} in dominantly octahedral sites which do not exclude Fe^{3+} in lower coordination number. These findings are consistent with earlier Mössbauer studies of iron phosphate glasses.[20,23,50] The corresponding parameters, isomer shift $\delta = 1.18$ mm s^{-1} and quadrupole splitting $\Delta = 2.25$ mm s^{-1} for Fe^{2+} and two for Fe^{3+} sites of $\delta = 0.38$ mm s^{-1} and $\delta = 0.37$ mm s^{-1} as well as of $\Delta = 1.00$ mm s^{-1} and $\Delta = 0.56$ mm s^{-1} are observed for F40 glass. The difference in Δ for Fe^{3+} ions in two sites is related to the higher environmental disorder of more intense site of Fe^{3+}. It is worth noting that the spectra of glass-ceramic heat-treated at 590°C show a slightly lower fraction of Fe^{2+} having a value of 14%.

With increasing temperature to 620°C along with three doublets for Fe^{2+} and Fe^{3+}, a new doublet having parameters $\delta = 1.20$ mm s^{-1} and $\Delta = 4.36$ mm s^{-1} appear in the Mössbauer spectrum. Such a high value of quadrupole splitting corresponds to the trigonal prismatic coordination of Fe^{2+} ions characteristic for $Fe_3(P_2O_7)_2$ crystalline phase. This crystalline phase is formed in the entire temperature range 620-700°C as confirmed by PXRD. Furthermore, Mössbauer spectrum for glass-ceramic heat-treated at 620°C was analyzed by the superposition of five doublets attributed to Fe^{2+} and Fe^{3+} ions in both glass matrix (three doublets) and $Fe_3(P_2O_7)_2$ crystalline phase (two doublets). The difference between Fe^{2+} ions in $Fe_3(P_2O_7)_2$ phase and residual glass matrix is visible in two doublets having values of quadrupole splitting, $\Delta = 2.37$ mm s^{-1} and $\Delta = 4.36$ mm s^{-1}, which corresponds to two different Fe^{2+} sites, one in octahedral (glass matrix) and the other one in trigonal prism ($Fe_3(P_2O_7)_2$ phase), Table 1.

TABLE 1 Hyperfine parameters determined from the fitting of the spectra for F40 glass and glass-ceramics heat-treated at various temperatures between 590 and 750°C for 24 h

Sample	δ/mm s^{-1}	ΔE_Q/mm s^{-1}	Γ/mm s^{-1}	Iron ion site	Relative area/%	Attributed phase	Fe^{2+}/Fe_{total}
Glass 16_F40	1.18	2.24	1.10	Fe^{2+}	16	Amorphous phase	0.16
	0.38	1.00	0.40	Fe^{3+}– site I	55		
	0.37	0.56	0.32	Fe^{3+}– site II	29		
@590	1.16	2.37	1.10	Fe^{2+}	15	Amorphous phase	0.14
	0.38	1.03	0.41	Fe^{3+}– site I	54		
	0.38	0.57	0.34	Fe^{3+}– site II	31		
@620	1.18	2.24	1.00	Fe^{2+}	9	Amorphous phase	0.12
	0.38	1.00	0.40	Fe^{3+}– site I	50		
	0.37	0.56	0.35	Fe^{3+}– site II	33		
	1.20	4.36	0.23	Fe^{2+}	3	$Fe_3(P_2O_7)_2$	
	0.40	0.51	0.40	Fe^{3+}	5		
@650	—	—	—	Fe^{2+}	—	Amorphous phase	0.13
	0.38	1.00	0.40	Fe^{3+}– site I	36		
	0.37	0.56	0.35	Fe^{3+}– site II	21		
	1.20	4.34	0.30	Fe^{2+}	13	$Fe_3(P_2O_7)_2$	
	0.46	0.30	0.30	Fe^{3+}	30		
@700	—	—	—	Fe^{2+}	—	Amorphous phase	0.13
	0.38	1.00	0.40	Fe^{3+}– site I	35		
	0.37	0.56	0.35	Fe^{3+}– site II	24		
	1.20	4.34	0.30	Fe^{2+}	13	$Fe_3(P_2O_7)_2$	
	0.45	0.27	0.30	Fe^{3+}	28		
@750	—	—	—	Fe^{2+}	—	Amorphous phase	0.13
	0.38	1.00	0.40	Fe^{3+}– site I	34		
	—	—	—	Fe^{3+}– site II	—		
	1.20	4.34	0.30	Fe^{2+}	14	$Fe_3(P_2O_7)_2$	
	0.44	0.28	0.30	Fe^{3+}	26		
	0.42	0.66	0.30	Fe^{3+}	16	$Fe_4(P_2O_7)_3$	
	0.34	0.42	0.35	Fe^{3+}	10	$Fe(PO_3)_3$	

Note: The estimated error in $<\delta>$, $<\Delta E_Q>$, and $<\Gamma>$ is ±0.01 mm/s. The isomer shifts are referenced to α-Fe at RT.

TABLE 2 Hyperfine parameters determined from the fitting of the spectra for glass-ceramics heat-treated at 800 and 830°C for 24 hours

Sample	δ/μμ s^{-1}	ΔE_Q/mm s^{-1}	Γ/mm s^{-1}	Iron ion site	Relative area/%	Attributed phase	Fe^{2+}/Fe_{tot}
@800	—	—	—	Fe^{2+}	—	Amorphous phase	0.12
	0.38	1.00	0.40	Fe^{3+}– site I	4		
	—	—	—	Fe^{3+}– site II	—		
	1.20	4.34	0.30	Fe^{2+}	12	$Fe_3(P_2O_7)_2$	
	0.50	0.38	0.35	Fe^{3+}	28		
	0.42	0.66	0.30	Fe^{3+}	36	$Fe_4(P_2O_7)_3$	
	0.34	0.42	0.35	Fe^{3+}	19	$Fe(PO_3)_3$	
	0.29	0.59	0.30	Fe^{3+}	1	$FePO_4$	
@830	—	—	—	Fe^{2+}	—	Amorphous Phase	0.11
	0.38	1.00	0.40	Fe^{3+}– site I	10		
	—	—	—	Fe^{3+}– site II	—		
	1.20	4.34	0.30	Fe^{2+}	11	$Fe_3(P_2O_7)_2$	
	0.50	0.38	0.30	Fe^{3+}	24		
	0.42	0.66	0.30	Fe^{3+}	35	$Fe_4(P_2O_7)_3$	
	0.34	0.42	0.35	Fe^{3+}	19	$Fe(PO_3)_3$	
	0.29	0.59	0.30	Fe^{3+}	1	$FePO_4$	

Note: The estimated error in <δ>, <ΔE_Q> and <Γ> is ±0.01 mm/s. The isomer shifts are referenced to α-Fe at RT.

As the crystallization temperature increases to 650 and 700°C, the shape of Mössbauer spectra is changed due to an increase in the amount of $Fe_3(P_2O_7)_2$ phase. In fact, doublet related to Fe^{2+} ions in the glass matrix disappears indicating a decrease in the amount of Fe^{2+} whereas doublet for Fe^{2+} ions in $Fe_3(P_2O_7)_2$ phase becomes more intense. On the other hand, quadrupole splitting values for Fe^{3+} ions in glass-ceramics heat-treated at 650 and 700°C decrease to $\Delta = 0.30$ and $\Delta = 0.27$ suggesting a less distorted local environment around the octahedral Fe^{3+} sites. Deformation of the central doublets in Mössbauer spectra is attributed to the Fe^{3+} ions in the glassy and crystalline phase.

Crystallization in the temperature range 750-830°C, see Figure 3B, leads to further changes in the glass-ceramic structures, that is, to the formation of the new crystalline phases, a dominant $Fe_4(P_2O_7)_3$ and $Fe(PO_3)_3$. It is evident that the fraction of Fe^{3+} in the glassy phase decreases and finally disappears with the progress of crystallization. Moreover, along with two doublets for Fe^{2+} and Fe^{3+} in $Fe_3(P_2O_7)_2$, every newly formed crystalline phase shows a characteristic contribution observed in Mössbauer spectra. According to literature, the $Fe_4(P_2O_7)_3$ phase contains four Fe^{3+} sites[47] while three Fe^{3+} sites are found for $Fe(PO_3)_3$ phase[51], Tables 1 and 2.

Mössbauer parameters for Fe^{3+} ions in $Fe_4(P_2O_7)$ are $\delta = 0.42$ and $\Delta = 066$ mm s^{-1}, whereas for Fe^{3+} ions in the $Fe(PO_3)_3$ the values are $\delta = 0.34$ and $\Delta = 0.42$ mm s^{-1}. This is consistent with literature data[49,51] confirming that the Fe^{3+} ions in these phases are situated in distorted octahedral coordination. At the same time, two doublets that correspond to the Fe^{2+} and Fe^{3+} in $Fe_3(P_2O_7)_2$ crystalline phase with a characteristic high value of quadrupole splitting for Fe^{2+}, $\Delta = 4.34$ mm s^{-1} are also present in the Mössbauer spectra.

Furthermore, higher values of $\delta = 0.50$ mm s^{-1} and $\Delta = 0.42$ mm s^{-1} for Fe^{3+} in $Fe_3(P_2O_7)_2$ phase is attributed to the increase in environmental disorder around Fe^{3+} ions as crystallization progresses. Concomitantly, for glass-ceramics heat-treated at 800 and 830°C, the deformation of the central doublets that correspond to the Fe^{3+} in the new crystalline phases formed becomes smaller since both $Fe_4(P_2O_7)_3$ and $Fe(PO_3)_3$ crystalline phases contain only Fe^{3+} ions. It is worth noting that during crystallization processes and increasing heat-treatment temperatures for all glass-ceramics investigated, there is no considerable change in the overall Fe^{2+}/Fe_{tot} ratio, that is, fraction of Fe^{2+} (changes only from 16% to 11%) as listed in Tables 1 and 2. As a conclusion, the evolution of Mössbauer spectra along with PXRD analysis clarify structural modifications and determine Fe^{3+} and Fe^{2+} ions coordination in both glassy and crystalline phases. The step in which the amount of Fe^{3+} and Fe^{2+} ions in each phase, glassy and crystalline, is specified plays a key role in further study of electrical properties of these pure polaronic glass-ceramics. Such a detailed analysis of Mössbauer spectra allows the identification of every Fe^{3+} and Fe^{2+} site and their significance in the electrical conductivity changes.

3.1.3 | Electrical properties of iron phosphate glass-ceramics

The effect of structural modifications induced by crystallization on the electrical conductivity spectra of

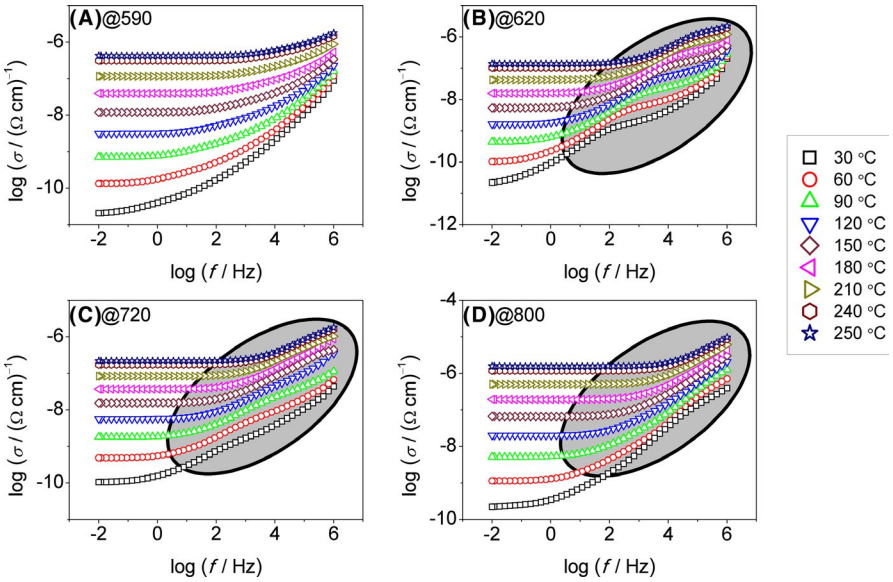

FIGURE 4 Conductivity spectra measured at various temperatures for F40-48 glass-ceramics prepared at (A) 590, (B) 620, (C) 720, and (d) 800°C

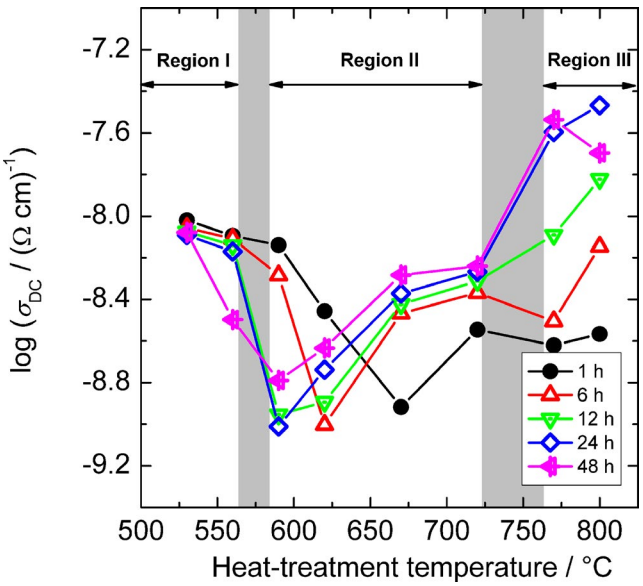

FIGURE 5 DC conductivity at 120°C for F40 glass-ceramics prepared at different heat-treatment temperatures and times

glass-ceramics prepared by heat treatments at 590, 620, 720, and 800°C for 48 hours is shown in Figure 4. For F40-48@590 sample, the conductivity spectra show two typical features; a plateau at a low frequency that corresponds to the DC conductivity, σ_{DC}, and a dispersion at higher frequencies which is related to the short-range polaronic transport within an amorphous glass network. With the increase in heat-treatment temperature, the shape of conductivity dispersion changes. According to the PXRD and analysis of Mössbauer spectra, heat treatments up to 720°C yield glass-ceramics which contain one $Fe_3(P_2O_7)_2$ phase whereas heat treatments at higher temperatures, 770-800°C, produce multiphase systems comprising three crystalline phases $Fe_3(P_2O_7)_2$, $Fe_4(P_2O_7)_3$, $Fe(PO_3)_3$, and glass matrix. Therefore, the observed changes in the shape of conductivity spectra can be related to a gradual formation of the abovementioned crystalline phase(s). Similar spectral features which emerged as a result of the progressed crystallization were also observed for glass-ceramics prepared at other heat-treatment times.

For all obtained glass-ceramics the DC conductivity, σ_{DC}, exhibits an Arrhenius temperature dependence with the characteristic activation energies for DC conductivity, W_{DC}, which can be determined from the relation: $\sigma_{DC} = \sigma_0 \exp(-W_{DC}/k_B T)$, where k_B is Boltzmann constant and T is the temperature. The values of σ_{DC}, W_{DC}, and σ_0 for F40 glass-ceramics prepared at different temperatures for 1 and 6 hours are listed in Table S1. A detailed discussion on the changes in W_{DC} with crystallization of F40 glass is given in the following section.

To understand the impact of heat-treatment duration on polaronic transport, the trends of σ_{DC} for all glass-ceramics are exhibited in Figure 5. As can be seen from the figure, three regions can be identified. The first region which is attributed to the lowest crystallization temperatures, <560°C, shows slight changes in σ_{DC} due to an early beginning of the crystallization. In the temperature region 590-720°C, here denoted as region II, σ_{DC} changes nonmonotonically: first showing a sharp decrease and then an increase with increasing heat-treatment temperature. The minimum in σ_{DC} shifts to lower temperature as crystallization time increases from 1 to 48 h. It is interesting to note that the lowest value of $\sigma_{DC} \approx 1 \times 10^{-9}$ $(\Omega\ cm)^{-1}$ is observed for the glass-ceramics in which the relative amount of crystalline $Fe_3(P_2O_7)_2$ phase is 8-15 wt% (F40-6@620, F40-12@590, F40-24@590), compare Figures 2 and 5. On the other hand, the magnitude of minimum in σ_{DC} is higher for F40-48 series, that is, for F40-48@560 glass-ceramic in which the amount of $Fe_3(P_2O_7)_2$ phase is 33 wt%.

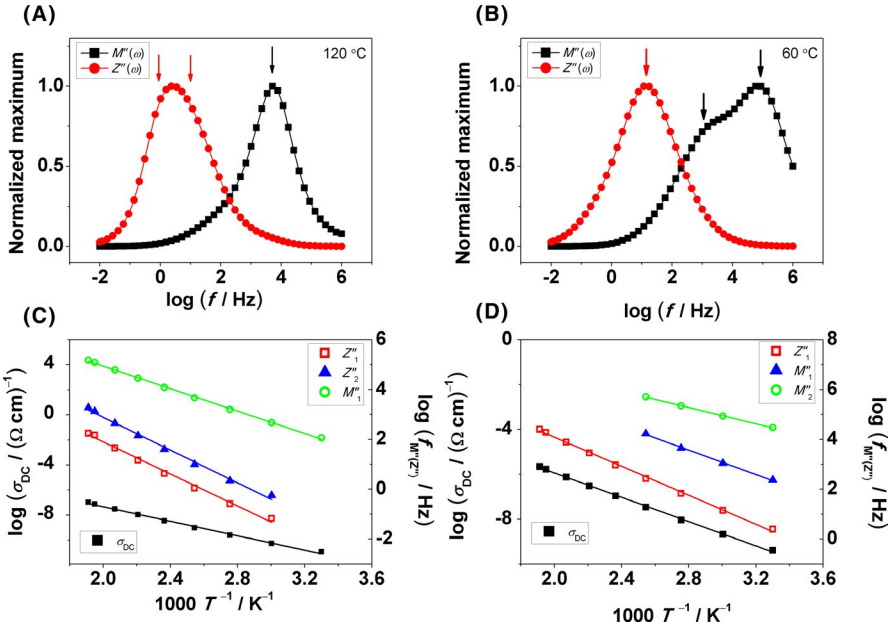

FIGURE 6 Frequency dependence of the normalized $M''(\omega)$ and $Z''(\omega)$ for F40-24 glass-ceramics heat-treated at (A) 590°C and (B) 800°C. Dependence of DC conductivity, log σ_{DC}, and relaxation frequencies, log $f_{M'',Z''}$, upon $1/T$, for F40-24 glass-ceramics heat-treated at (C) 590°C and (D) 800°C

These results indicate that the growth of $Fe_3(P_2O_7)_2$ phase within the glassy matrix has a dual role in the polaronic transport. First, the sharp decrease in the σ_{DC} is a result of the impoverishment of the concentration of Fe^{2+}-Fe^{3+} pairs in the dominant glass matrix.[27] Second, the increase in σ_{DC} with further increase in crystallization temperature up to 720°C is due to the increase of the amount of well-defined $Fe_3(P_2O_7)_2$ phase to ≈38-40 wt% for F40-24 and F40-48 glass-ceramics. Here, it can be inferred that a better connection of crystalline grains, and, hence, the formation of easier conduction pathways enhances the polaron mobility between Fe^{2+}-Fe^{3+} pairs through and along $Fe_3(P_2O_7)_2$ crystallites.

In the third temperature region, 770-800°C, an additional increase in the σ_{DC} is observed as new $Fe_4(P_2O_7)_3$ and $Fe(PO_3)_3$ phases are formed. An enhancement in σ_{DC} for glass-ceramics crystallized for 24 and 48 hours can be explained by the formation of conduction pathways through different crystalline grains that have similar structures. In our previous paper,[27] we have reported that in $Fe_4(P_2O_7)_3$ phase, which contains only Fe^{3+} ions, the phosphate dimmers along *a* axis form empty prism which is similar to trigonal prismatic coordination of Fe^{2+} in $Fe_3(P_2O_7)_2$ phase. Thus, the intertwining of similar structures of dominant single valence $Fe_4(P_2O_7)_3$ and conductive mixed valence $Fe_3(P_2O_7)_2$ enables the formation of continuous conduction pathways for uninterrupted polaron transport through both phases.

3.1.4 | Electrical relaxation and activation energies

As mentioned in the previous section, the occurrence of the crystalline phases in glass-ceramics causes visible changes in the shape of the conductivity spectra, see Figure 4. However, it is not possible to extract information on the electrical processes within different phases (crystalline/glassy) in glass-ceramics from the conductivity spectra. Hence, we attempt to identify them and separate their contributions to the overall electrical conductivity by analyzing relaxation processes detectable in the frequency dependence of imaginary part of impedance, $Z''(\omega)$ and electrical modulus, $M''(\omega)$. The complex electric modulus $M^*(\omega)$ is defined as an inverse of complex permittivity, ε^*: $M^*(\omega) = 1/\varepsilon^* = \varepsilon'/((\varepsilon')^2 + (\varepsilon'')^2) + j\varepsilon''/((\varepsilon')^2 + (\varepsilon'')^2) = M'(\omega) + jM''(\omega)$, where $j = \sqrt{-1}$. This formalism suppresses the contribution of the DC conductivity and electrode polarization effects which dominate at lower frequencies.

It is well known that the spectra of $M''(\omega)$ and $Z''(\omega)$ may show one or more maxima depending on the presence of different phases within a material. The characteristic frequency of each maximum in $M''(\omega)$ and $Z''(\omega)$, $f_{M''}$ and $f_{Z''}$, is related to the relaxation time, $\tau_{M''}$ and $\tau_{Z''}$ via relation $f_{M'',Z''} = 1/(2\pi\tau_{M'',Z''})$.[52] It should be pointed out that the $M''(\omega)$ spectra are dominated by the processes with small capacitance whereas $Z''(\omega)$ spectra are related to the processes with high resistivity values.

Figure 6 shows the spectra of normalized $M''(\omega)$ and $Z''(\omega)$ for F40-24 glass-ceramics prepared at (A) 590°C and (B) 800°C. Considering the relaxation processes in F40-24@590 glass-ceramics, it can be seen that $Z''(\omega)$ shows a broad slightly asymmetric peak indicating two relaxation processes, whereas $M''(\omega)$ exhibits a single peak located at much higher frequencies. The two contributions in the $Z''(\omega)$ spectrum which are related to the $Fe_3(P_2O_7)_2$ phase and grain boundaries, respectively, are separated using the nonlinear least square method with Lorentzian function approximation and their characteristic relaxation frequencies, $f_{Z''CP1}$ and $f_{Z''gb}$, are

Sample	Region	W_{DC}/eV	W_{gm}/eV	W_{CP1}/eV	W_{CP2}/eV	W_{gb}/eV
F40 glass	—	0.62	0.62	—	—	—
F40-24@530	(I)	0.62	0.62	—	—	—
F40-24@560		0.63	0.65	0.63	—	—
F40-24@590	(II)	0.57	0.45	0.65	—	0.64
F40-24@620		0.52	0.45	0.55	—	0.55
F40-24@670		0.49	0.45	0.51	—	0.54
F40-24@720		0.48	0.44	0.52	—	0.54
F40-24@770	(III)	0.54	—	0.49	0.33	0.60
F40-24@800		0.54	—	0.49	0.32	0.58

TABLE 3 Activation energy of total DC conductivity, W_{DC}, and activation energies for each particular contribution (glass matrix, crystal phases and grain boundary) for F40-24 glass-ceramics

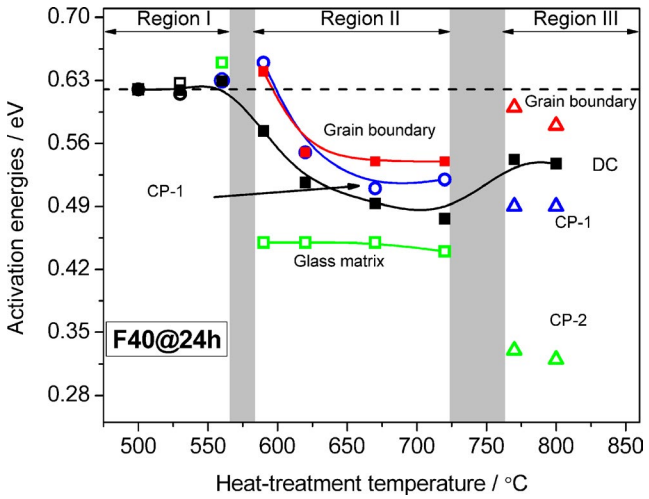

FIGURE 7 Dependence of activation energy of total DC conductivity, W_{DC}, and activation energies for each contribution to the total electrical conductivity (glass matrix, crystal phases, and grain boundary) on the heat-treatment temperature for F40-24 glass-ceramics

determined. It is important to note that these two maxima are nearly overlapped indicating close relaxation times of contributions from crystalline $Fe_3(P_2O_7)_2$ and grain boundary. These results are consistent with our previous study[27] where the resistivity values of $Fe_3(P_2O_7)_2$ crystalline phase and grain boundaries are of the same order of magnitude, $\approx 3 \times 10^7\ \Omega$ and $\approx 7 \times 10^7\ \Omega$, respectively.

On the other hand, the maximum in $M''(\omega)$ observed at much higher frequencies corresponds to the phase with the lowest value of capacitance and is attributed to the dominant glassy phase. Here, it should be mentioned that the contribution of the glass matrix cannot be resolved from the complex impedance plot[27] but using electric modulus formalism. From this formalism, the characteristic relaxation frequency for the glassy phase in F40-24@590 glass-ceramic can be easily identified and determined, see Figure 6A.

With increasing heat-treatment temperature to 800°C, the $M''(\omega)$ and $Z''(\omega)$ spectra behave differently when compared with the previous sample, showing two maxima in $M''(\omega)$ at high and intermediate frequencies and one maximum in $Z''(\omega)$ at low frequencies, see Figure 6B. The two distinguished maxima in $M''(\omega)$ correspond to the relaxation processes in dominant $Fe_4(P_2O_7)_3$ (higher frequency) and $Fe_3(P_2O_7)_2$ (lower frequency) phases, whereas maximum in $Z''(\omega)$ is related to the process with higher relaxation time associated with grain boundaries. Figure 6C,D represents an Arrhenius plot for σ_{DC} and relaxation frequencies, $f_{M''1}$, $f_{M''2}$, $f_{Z''1}$, and $f_{Z''2}$ from which the activation energies for each contribution, that is, glass matrix, $Fe_3(P_2O_7)_2$ and $Fe_4(P_2O_7)_3$ crystalline phases and grain boundaries are calculated and summarized in Table 3.

Figure 7 exhibits the dependence of the activation energy of overall DC conductivity, W_{DC}, and activation energies of different relaxation processes determined using $M''(\omega)$ and $Z''(\omega)$ spectra on the crystallization temperature for F40-24 glass-ceramics. In the temperature region I, the W_{DC} is almost constant at about 0.62 eV. However, close inspection shows that at 560°C, the activation energy related to the glass matrix, W_{gm}, slightly increases to 0.65 eV indicating an early beginning of the formation of the first $Fe_3(P_2O_7)_2$ phase.

In the transition from the region I to region II, the W_{DC} starts to decrease. At the same time, three contributions to the overall conductivity could be distinguished and their activation energies could be determined; W_{gm} for the glass matrix, W_{CP1} for the $Fe_3(P_2O_7)_2$ phase and W_{gb} for the grain boundaries, see Table 3 and Figure 7. The values of W_{CP1} and W_{gb} are similar $\approx$0.65 eV and are higher than $W_{DC} = 0.57$ eV. However, the values of W_{gm} for glass matrix are found to be unexpectedly low $\approx$0.45 eV in the entire temperature region II.

With increasing heat-treatment temperature, in the region II, the fraction of $Fe_3(P_2O_7)_2$ phase increases causing a decrease in W_{DC} down to the plateau of 0.48 eV. Moreover, for F40-24@720 glass-ceramics, the activation energies

W_{CP1} and W_{gb} reveal an identical trend, having higher values 0.52 eV and 0.54 eV, respectively. This result agrees well with the PXRD analysis which showed that a two-phase system comprising glass matrix and $Fe_3(P_2O_7)_2$ crystalline phase, exists in region II. Besides, it seems that the activation energy for glass matrix, W_{gm}, is independent of the heat-treatment temperatures.

The transition from region II to region III is accompanied by an increase in W_{DC} indicating additional structural changes. The three contributions present here, and their activation energies, W_{CP2}, W_{CP1} and W_{gb}, are related to the $Fe_4(P_2O_7)_3$, $Fe_3(P_2O_7)_2$ phases and grain boundaries, respectively. In region III, the fraction of glass matrix reduces significantly and $Fe_4(P_2O_7)_3$ becomes a dominant crystalline phase.[27] Therefore, it can be concluded that the formation of $Fe_4(P_2O_7)_3$ phase causes a steep increase in σ_{DC} as shown in Figure 5. Indeed, the corresponding activation energy, $W_{CP2,}$ determined for glass-ceramics prepared at 770 and 800°C shows the lowest values equal to 0.33 and 0.32 eV, respectively. The contribution of $Fe_3(P_2O_7)_2$ phase which appears as a second maximum in $M''(\omega)$, Figure 6B, exhibits activation energy of ≈0.49 eV which is slightly lower than that of W_{CP1} ≈0.52 eV in the region II. Both W_{CP1} and W_{CP2} values are lower than the activation energy for overall DC conductivity, W_{DC}. The reason for higher W_{DC} value lies in the high activation energy of grain boundaries, W_{gb}, with a value of ≈0.60 eV. It could be concluded that in the multiphase systems obtained at high heat-treatment temperatures, region III, the formation of continuous grain boundaries along different crystalline grains is responsible for high W_{gb}. Thus, the high activation energy of grain boundaries acts as a limiting factor for the overall electrical transport. Nevertheless, the facilitating role of easy conductive pathways through the crystalline phases ($Fe_4(P_2O_7)_3$ in particular) prevails the limiting role of the grain boundary and these highly crystalline multiphase systems exhibit highest DC conductivity among all F40 glass-ceramics, see Figure 5.

3.2 | Predominantly polaron conductive glass-ceramics

3.2.1 | Structural characterization of lithium tungsten glass-ceramics (Li-50W)

Structural changes induced by the heat treatments of Li-50W glass at 600, 725, and 800°C for 6 hours are exhibited in Figure 8. PXRD patterns for Li-50W@600 and Li-50W@725 samples show no diffraction lines which indicate their amorphous structure. However, as can be seen from the SEM micrograph of Li-50W@600 sample, see Figure S4A, well-defined dendritic microstructures related to an initial stage of crystallization are present on the surface of this system. At crystallization temperature

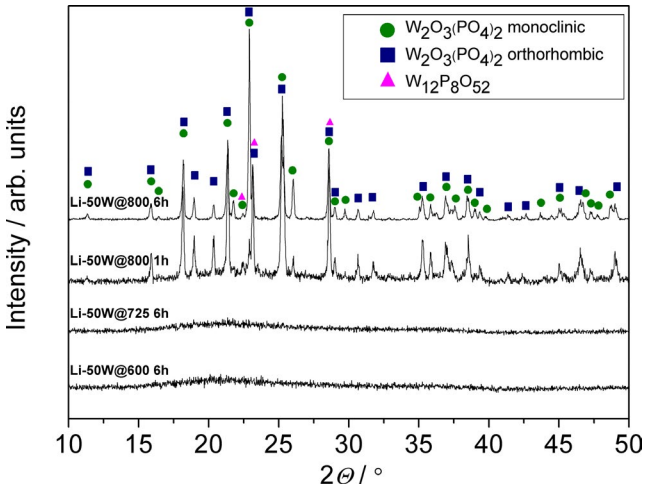

FIGURE 8 PXRD patterns of Li-50W glass-ceramics prepared at various temperatures for 1 and 6 h

of 800°C, the diffraction lines corresponding to the two polymorphs of $W_2O_3(PO_4)_2$, orthorhombic (ICSD no: 50 742) and monoclinic (ICSD no: 24 072), appear in the PXRD pattern. Some barely detectable lines of $W_{12}P_8O_{52}$ (ICSD no: 24 832) can also be found in this pattern. To gain a better insight into the formation of crystalline phases for this sample, we have crystallized Li-50W glass at the same temperature, 800°C, but only for 1 hour. The PXRD pattern of this sample is also displayed in Figure 8. Interestingly, it seems that all three phases also crystallize when heat treatment lasts for 1 hour and prolonging the heat-treatment time to 6 hours only causes their further simultaneous growth. However, as can be seen from the SEM micrograph in Figure S4B, in the Li-50W glass-ceramic prepared at 800°C for 6 hours along with well-defined $W_2O_3(PO_4)_2$ crystals, a large amount of about 50 wt% of glass matrix is still present despite the high crystallization temperature and relatively long heating time. This is in line with the fact that glasses containing a lower amount of WO_3 and higher alkali content do not crystallize.

It should be noted that both $W_2O_3(PO_4)_2$ polymorphs contain tungsten ions in the W^{6+} oxidation state and their structure is built up from corner-sharing PO_4 tetrahedra and WO_6 octahedra, where two WO_6 octahedra are linked together through a bridging oxygen atom to form a W_2O_{11} dioctahedral unit.[53] Without going into further details, the main structural difference between the two polymorphic forms is evident in the two terminal W-O bonds arranged in different directions. From the point of view of electrical investigations of glass-ceramics, to identify the contributions of such structurally similar crystalline phases in the overall conduction process is a challenging task.

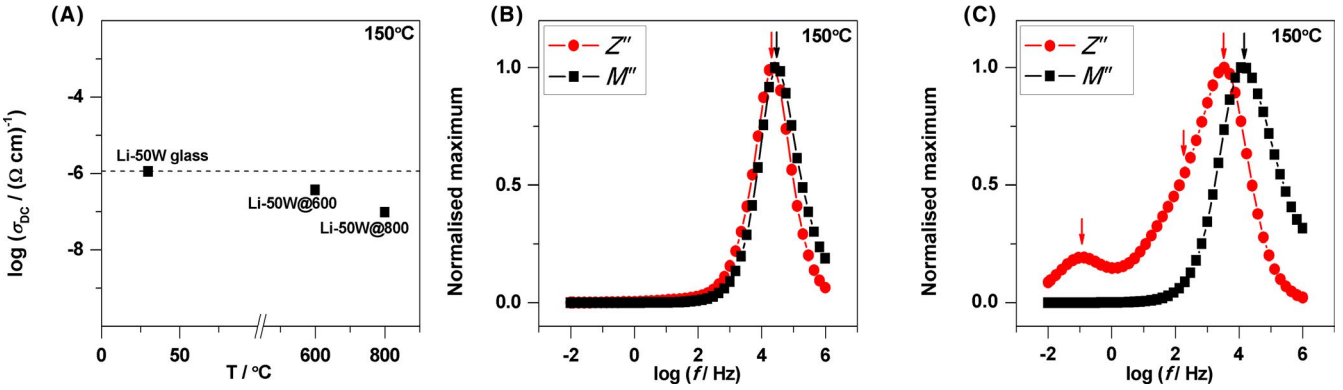

FIGURE 9 (A) DC conductivity measured at 150°C for Li-50W glass and glass-ceramics. Normalized $Z''(\omega)$ and $M''(\omega)$ measured at 150°C for (B) Li-50W@600 and (C) Li-50W@800 glass-ceramics

3.2.2 | Electrical properties

Conductivity spectra for Li-50W@600 sample shown in Figure S5, illustrate the typical spectra for polaronic glasses showing long σ_{DC} plateau at low frequencies and dispersion at high frequencies. For Li-50W@800 glass-ceramics, changes in the shape of conductivity spectra, which get more pronounced with increasing temperature, are related to the formation of $W_2O_3(PO_4)_2$ crystalline phases. The obtained values of activation energy for DC conductivity, W_{DC}, for Li-50W@600 and Li-50W@800 samples are 0.49 and 0.52 eV, respectively, whereas for parent Li-50W glass W_{DC} is found to be 0.45 eV.

Figure 9A shows the dependence of σ_{DC} measured at 150°C on the crystallization temperatures. The values for σ_{DC} are 3.4×10^{-7} $(\Omega\ \text{cm})^{-1}$ and 1×10^{-7} $(\Omega\ \text{cm})^{-1}$ for Li-50W@600 and Li-50W@800, respectively, which is just slightly lower than σ_{DC} of nontreated parent glass. Thus, it seems that the σ_{DC} is nearly independent of the heat treatments, that is, the formation of $W_2O_3(PO_4)_2$ crystalline phases. While both $W_2O_3(PO_4)_2$ polymorphs contain tungsten in W^{6+} oxidation state, the W^{5+}-W^{6+} pairs which remain in the residual glassy phase play an important role in keeping the mobility of polarons, and hence σ_{DC} remains almost unchanged. As mentioned earlier, for Li-50W glass, the W^{5+}/W_{tot} fraction is relatively low, 1.26%. However, it was previously reported[31] that despite such a low W^{5+} concentration, Li-50W glass exhibits very high polaronic conductivity. Thus, it is likely that a slight decrease in the number of W^{5+}-W^{6+} pairs in the glassy phase due to a formation of crystalline phases is responsible for a slight decrease in σ_{DC} of Li-50W glass-ceramics.

Considering the composition of the parent Li-50W glass, it can be argued that a small concentration of Li^+ ions (5 mol%) might have some impact on the electrical conductivity of Li-50W glass-ceramics. However, we have previously reported[31] that the dominant conduction mechanism in Li-50W glass is polaronic and since there are no significant changes in σ_{DC} for the obtained glass-ceramics, it can be concluded that in these materials, the polaronic transport through the glassy phase has a key role.

Another aspect of the analysis of the electrical properties of Li-50W glass-ceramics is the evaluation of the relaxation times using the frequency response of $Z''(\omega)$ and $M''(\omega)$. As mentioned earlier, the $Z''(\omega)$ and $M''(\omega)$ spectra are suitable for the identification of the resistive component and the component having high capacitance, respectively.

Figure 9B exhibits the normalized $Z''(\omega)$ and $M''(\omega)$ spectra for Li-50W@600 sample showing practically overlapped peaks suggesting that both bulk responses, that is, localized relaxation and nonlocalized conductivity, are due to the same relaxation process. This behavior implies that after heat treatment at 600°C, the electrical relaxation occurs within a dominant glassy phase in a very similar manner as in the parent Li-50W glass. This is in a good agreement with PXRD analysis and SEM microscopy, see Figure 8 and Figure S4. On the other hand, with increasing crystallization temperature to 800°C, the three maxima in $Z''(\omega)$ and one maximum in $M''(\omega)$ spectrum are determined, see Figure 9C. The relaxation frequencies and activation energies calculated from each maximum in $Z''(\omega)$ and $M''(\omega)$ spectra for Li-50W@600 and Li-50W@800 samples are listed in Table S2a,b.

Comparable values of the relaxation frequency, $f_{Z''} = 2.0 \times 10^4$ Hz and $f_{M''} = 3.2 \times 10^4$ Hz, for Li-50W@600 sample confirm a single relaxation process which corresponds to the glass matrix. In contrast, for Li-50W@800 glass-ceramics, the three contributions are separated from $Z''(\omega)$ spectrum. The first relaxation, at the lowest frequency, is related to the grain boundaries having a value of activation energy, $W_{gb} = 0.65$ eV. The second barely detectable relaxation at a higher frequency is probably connected to the formation of one of the $W_2O_3(PO_4)_2$ polymorphs with $W_{Cg1} = 0.54$ eV. The most intense $Z''(\omega)$ maximum at even higher frequencies shows activation energy of $W_{Cg2} = 0.63$ eV and could be attributed to another $W_2O_3(PO_4)_2$ polymorph with higher wt%

than the first one. To be able to unambiguously ascertain each of the polymorphs to their corresponding relaxation maxima, a further structural (quantitative) analysis is needed as well as the investigation of this glass-ceramic system with a wider fraction of crystalline/glassy phases. This study is underway.

Finally, a single relaxation visible in $M''(\omega)$ spectrum pertains to the process within the glassy matrix and is characterized by the activation energy, $W_{gm} = 0.52$ eV. This value is close to the activation energy for DC conductivity of parent Li-50W glass, $W_{DC} = 0.45$ eV, which supports the conclusion that the glass matrix contribution in Li-50W@800 glass-ceramic is significant.

4 | CONCLUSION

The influence of controlled crystallization on the electrical transport of pure polaron conductive $40Fe_2O_3$-$60P_2O_5$ (mol%), F40, and predominantly polaronic $5Li_2O$-$5ZnO$-$40P_2O_5$-$50WO_3$ (mol%), Li-50W, glasses was investigated by varying heat-treatment temperature and time. In F40 glass-ceramics prepared at lower heat-treatment temperatures, up to ≈720°C, the only crystalline phase formed is $Fe_3(P_2O_7)_2$ whereas at higher temperatures ≈800°C, another two phases, $Fe_4(P_2O_7)_3$ and $Fe(PO_3)_3$, appeared. However, these structural modifications observed upon crystallization processes strongly depend on crystallization times. The emergence of crystalline phase(s) recorded by Mössbauer spectroscopy is followed by the changes in Fe^{3+} and Fe^{2+} sites typical for each phase, crystalline or glassy. This allows us to identify the significance of different iron sites in the electrical conductivity changes. The strong dependence of electrical conductivity of F40 glass-ceramics on their structural modifications induced by crystallization is directly observed from the DC conductivity and frequency dependence of $Z''(\omega)$ and $M''(\omega)$. The activation energy of the overall conductivity of the samples obtained at low crystallization temperatures up to 590°C is almost constant, at about 0.62 eV, suggesting a single process related to the glass matrix. Furthermore, in the temperature range between 590 and 620°C the abrupt decrease in the electrical conductivity for all glass-ceramics heat-treated for various times is a result of the decrease in the Fe^{2+}-Fe^{3+} pairs concentration in the dominant glass matrix. The activation energies related to the $Fe_3(P_2O_7)_2$ crystallites and grain boundaries contributions in the temperature region up to ≈720°C decrease showing the same trend. Further increase in conductivity is associated with the formation of the well-defined $Fe_3(P_2O_7)_2$ crystals that enhance the Fe^{2+} -Fe^{3+} pairs polaron transport. Thus, this single crystalline phase system presents the lowest overall activation energy mainly related to the grain contribution. In the multiphased system at higher crystallization temperatures, the tendency and magnitude of the overall electrical conductivity are mostly limited by the grain boundary contribution.

The crystallization processes in Li-50W glass-ceramics are related to the formation of two polymorphs of $W_2O_3(PO_4)_2$ phase. DC conductivity slightly decreases upon crystallization due to the decrease in the concentration of W^{5+}-W^{6+} pairs in the residual glassy phase.

Considering the lack of significant change in σ_{DC} of glass-ceramics compared to predominantly polaron conducting starting glass, it can be concluded that the electrical transport in these crystallized glasses is also polaronic in nature and independent of Li^+ ions.

This work combines the course of crystallization processes and determination of each contribution to the overall electrical conductivity in F40 and Li-50W glass-ceramics. The structural modifications caused by induced crystallization have a key role in the polaronic transport mechanism in these two types of glass-ceramics.

ACKNOWLEDGMENTS

This work was supported by the Croatian Science Foundation; project IP-09-2014-5863. L. P. is grateful to the Croatian Science Foundation (03.01/156) for granting a doctoral fellowship which partially supported this work. The authors acknowledge the Ministry of Science, Education and Sport of the Republic of Croatia (grant no.: 098–0982929-2916) and PEst-C/CTM/LA0025/2011 (Portugal) for support. The authors are very grateful to Profs. L. Koudelka and P. Mošner for their assistance in the preparation of mixed ion-polaron glasses.

ORCID

Luka Pavić https://orcid.org/0000-0003-2232-6602
Andrea Moguš-Milanković https://orcid.org/0000-0001-6686-6470

REFERENCES

1. Deubener J, Allix M, Davis MJ, et al. Updated definition of glass-ceramics. J Non-Cryst Solids. 2018;501:3–10.
2. Zanotto ED. Bright future for glass-ceramics. J Non-Cryst Solids. 2018;501:3–10.
3. McMillan PW. Glass-Ceramics. New York: Academic Press; 1979.
4. Brow RK. The structure of simple phosphate glasses. J Non-Cryst Solids. 2000;263–264:1–28.
5. Sales BC, Boatner LA. Lead-iron phosphate glass: a stable storage medium for high-level nuclear waste. Science. 1984;226:45–8.
6. Day DE, Wu Z, Ray CS, Hrma P. Chemically durable iron phosphate glass wasteforms. J Non-Cryst Solids. 1998;241:1–12.
7. Yu X, Day DE, Long GJ, Brow RK. Properties and structure of sodium-iron phosphate glasses. J Non-Cryst Solids. 1997;215:21–31.
8. Fang X, Ray CS, Moguš-Milanković A, Day DE. Iron redox equilibrium, structure and properties of iron phosphate glasses. J Non-Cryst Solids. 2001;283:162–72.

9. Bridge B, Patel ND. Composition dependence of the infra-red absorption spectra molybdenum phosphate and some crystalline analogues. J Non-Cryst Solids. 1987;91:27–41.
10. Sayer M, Mansingh A. Transport properties of semiconducting phosphate glasses. Phys Rev B. 1972;6:4629.
11. Mott NF. Conduction in glasses containing transition metal ions. J Non-Cryst Solids. 1968;1:1–17.
12. Austin IG, Mott NF. Polarons in crystalline and non-crystalline materials. Adv Phys. 1969;18:41–102.
13. Murawski L, Chung CH, Mackenzie JD. Electrical properties of semiconducting oxide glasses. J Non-Cryst Solids. 1979;32:91–104.
14. Moguš-Milanković A, Day DE, Šantić B. DC conductivity and polarisation in iron phosphate glasses. Phys Chem Glasses. 1999;40:69–74.
15. Šantić A, Moguš-Milanković A. Charge carrier dynamics in materials with disordered structures: a case study of iron phosphate glasses. Croat Chem Acta. 2012;85:245254.
16. Sales BC, Boatner LA. Radioactive waste forms for the future. In: Lutze W, Ewing RC editors. Amsterdam: North-Holland, 1988; p. 193–231.
17. Jermoumi T, Hafid M, Niegisch N, Mennig M, Sabir A, Toreis N. Properties of $(0.5-x)Zn–xFe_2O_3–0.5P_2O_5$ glasses. Mater Res Bull. 2002;37:49–57.
18. Mesko MG, Day DE. Immobilization of spent nuclear fuel in iron-phosphate glass. J Nucl Mater. 1999;273:27–36.
19. Brow RK, Arens CM, Yu X, Day DE. XPS study of iron phosphate glasses. Phys Chem Glasses. 1994;35:132.
20. Marasinghe GK, Karabulut M, Ray CS, et al. Structural features of iron phosphate glasses. J Non-Cryst Solids. 1997;222:144–52.
21. Doupovec J, Sitek J, Kákoš J. Crystallization of iron phosphate glasses. J Therm Anal Calorim. 1981;22:213–9.
22. Moguš-Milanković A, Rajić M, Drašner A, Trojko R, Day DE. Crystallisation of iron phosphate glasses. Phys Chem Glasses. 1998;39:70–5.
23. Ray CS, Fang X, Karabulut M, Marasinghe GK, Day DE. Effect of melting temperature and time on iron valence and crystallization of iron phosphate glasses. J Non-Cryst Solids. 1999;249:1–16.
24. Pavić L, Graca M, Skoko Ž, Moguš-Milanković A, Valente MA. Magnetic properties of iron phosphate glass and glass-ceramics. J Am Ceram Soc. 2014;97:2517–24.
25. Moguš-Milanković A, Šantić A, Pavić L, Sklepić K. Iron phosphate glass-ceramics. Croat Chem Acta. 2015;88:553–60.
26. Moguš-Milanković A, Sklepić K, Skoko Ž, Mikac L, Musić S, Day DE. Influence of nanocrystallization on the electronic conductivity of zinc iron phosphate glass. J Am Ceram Soc. 2012;95:303–11.
27. Pavić L, Skoko Ž, Gajović A, Su D, Moguš-Milanković A. Electrical transport in iron phosphate glass-ceramics. J Non-Cryst Solids. 2018;502:44–53.
28. Poirier G, Messadeq Y, Ribeiro S, Poulain M. Structural study of tungstate fluorophosphate glasses by Raman and X-ray absorption spectroscopy. J Solid State Chem. 2005;178:1533–8.
29. De Araujo CC, Strojek W, Zhang L, et al. Structural studies of $NaPO_3–WO_3$ glasses by solid state NMR and Raman spectroscopy. J Mater Chem. 2006;16:3277–84.
30. Santagnelli SH, de Araujo CC, Strojek W, et al. Structural studies of $NaPO_3–MoO_3$ glasses by solid-state nuclear magnetic resonance and Raman spectroscopy. J Phys Chem B. 2007;111:10109–17.
31. Nikolić J, Pavić L, Šantić A, et al. Novel insights into electrical transport mechanism in ionic-polaronic glasses. J Am Ceram Soc. 2018;101:1221–35.
32. Pavić L, Šantić A, Nikolić J, et al. Nature of mixed electrical transport in Ag_2O-ZnO-P_2O_5 glasses containing WO_3 and MoO_3. Electrochim Acta. 2018;276:434–45.
33. Subbalakshmi P, Veeraiah N. Study of $CaO–WO_3–P_2O_5$ glass system by dielectric properties, IR spectra and differential thermal analysis. J Non-Cryst Solids. 2002;298:89–98.
34. Sambasiva Rao K, Srinivasa Reddy M, Ravi Kumar V, Veeraiah N. Dielectric, magnetic and spectroscopic properties of $Li_2O–WO_3–P_2O_5$ glass system with Ag_2O as additive. Mat. Chem. Phys. 2008;111:283–92.
35. Dyre C, Maas P, Roling B, Sidebottom DL. Fundamental questions relating to ion conduction in disordered solids. Rep Prog Phys. 2009;72:046501.
36. Martin SW. Ionic conduction in phosphate glasses. J Am Ceram Soc. 1991;74:1767–84.
37. Goodenough JB, Kim Y. Challenges for rechargeable Li batteries. Chem Mater. 2010;22:587–603.
38. Park M, Zhang X, Chung M, Less GB, Sastry AM. A review of conduction phenomena in Li-ion batteries. J Power Sources. 2010;195:7904–29.
39. Nitta N, Wu F, Lee JT, Yushin G. Li-ion battery materials: present and future. Mater Today. 2015;18:252–64.
40. Wang C, Hong J. Ionic/electronic conducting characteristics of $LiFePO_4$ cathode materials. Electrochem Solid-State Lett. 2007;10:A65–A69.
41. Ma J, Wang C, Wroblewski S. Kinetic characteristics of mixed conductive electrodes for lithium ion batteries. J Power Sources. 2007;164:849–56.
42. Riess I. Electrochemistry of mixed ionic-electronic conductors. In: Gellings PJ, Bouwmeester H editors. The CRC handbook of solid state electrochemistry. Boca Raton, FL:CRC Press, 1997.
43. Poirier G, Cassanjes FC, Messadeq Y, Ribeiro SJ. Crystallization of monoclinic WO_3 in tungstate fluorophosphate glasses. J Non-Cryst Solids. 2009;355:441–6.
44. Poirier G, de Araujo CC, Messadeq Y, Ribeiro SJ. Tungsten fluorophosphate glass as optical limiters. J Appl Phys. 2002;9:100221.
45. Poirier G, Nalin M, Messadeq Y, Ribeiro SJ. Photochromic properties of tungstate-based glasses. Solid State Ionics. 2007;178:871–5.
46. Mączka M, Kępiński L, Hanuza J, Kojima S. Studies of nanostructuring in cesium magnesium tungsten phosphate glass. J Non-Cryst Solids. 2007;353:4681–90.
47. Maddukuri S, Upadhyayula VV. Electrochemical lithium and sodium insertion studies on tungsten oxyphosphate. Chemistry Select. 2017;2:9186–92.
48. Ijjaali M, Venturini G, Gererdin R, Malaman B, Gleitzer C. Synthesis, structure and physical properties of a mixed-valence iron diphosphate $Fe_3(P_2O_7)_2$: first example of trigonal prismatic Fe^{2+} with O_2-ligands. Eur J Inorg Chem. 1991;28:983–98.
49. Elbouaanani LK, Malaman B, Gererdin R, Ijjaali M. Crystal structure refinement and magnetic properties of $Fe_4(P_2O_7)_3$ studied by neutron diffraction and mossbauer techniques. J Solid State Chem. 2002;163:412–20.
50. Ma L, Brow RK, Choudhury A. Structural study of $Na_2O–FeO–Fe_2O_3–P_2O_5$ glasses by Raman and Mössbauer spectroscopy. J Non-Cryst Solids. 2014;402:64–73.
51. Elbouaanani LK, Malaman B, Gerardin R. Structure refinement and magnetic properties of C-Fe $(PO_3)_3$ studied by neutron diffraction and Mössbauer techniques. J Solid State Chem. 1999;148:455–63.

52. Macedo PB, Moynhan CT, Rose R. The role of ionic diffusion in polarisation in vitreous ionic conductors. Phys Chem Glasses. 1972;13:171–9.
53. Hanawa M, Imoto H. Structures of Two new polymorphic forms of hexavalent tungsten oxide phosphates. J Solid State Chem. 1999;144:325–9.

SUPPORTING INFORMATION

Additional supporting information may be found online in the Supporting Information section at the end of the article.

How to cite this article: Pavić L, Nikolić J, Graça MPF, et al. Effect of controlled crystallization on polaronic transport in phosphate-based glass-ceramics. *Int J Appl Glass Sci*. 2020;11:97–111. https://doi.org/10.1111/ijag.13618